Pharm Res (2012) 29:2047–2059
DOI 10.1007/s11095-012-0732-6

RESEARCH PAPER

Structure and Function of Purified Monoclonal Antibody Dimers Induced by Different Stress Conditions

Rajsekhar Paul • Alexandra Graff-Meyer • Henning Stahlberg • Matthias E. Lauer • Arne C. Rufer • Hermann Beck • Alexandre Briguet • Volker Schnaible • Thomas Buckel • Sabine Boeckle

Received: 21 October 2011 / Accepted: 5 March 2012 / Published online: 5 April 2012

ABSTRACT

Purpose To investigate structure and function of different monoclonal antibody (MAb) dimers.

Methods MAb dimers were induced by process-related, low pH and UV light stress. Dimers were isolated and purified by chromatography and extensively characterized by biochemical, structural and functional methods.

Results Highly purified dimer forms were obtained which enabled detailed characterization. Dimers induced by process stress were associated by a single non-covalent interaction site between two Fab domains in a characteristic "bone-like" structure observed in Transmission Electron Microscopy (TEM). These dimers showed reduced potency and antigen binding affinity. Low pH stress generated more stable but also non-covalently associated dimers without chemical alterations in a typical "closed" conformation according to TEM. These dimer species were more compact and more hydrophobic as dimers induced by process stress. They showed bioactivity and antigen binding affinity similar to the native monomer. Light-induced dimers, exhibiting various different conformations, were the most stable dimers with various chemical modifications leading to a broad range in size, charge and hydrophobicity. These dimers fully lost bioactivity and antigen binding affinity.

Conclusion The use of highly purified MAb dimers and a panel of characterizations methods enabled to obtain a clear picture about molecular architecture and function of dimers.

KEY WORDS antibody dimer · function · monoclonal antibody · protein aggregation · structure

ABBREVIATIONS

AU	absorption units
AUC	analytical ultracentrifugation
CDR	complementarity-determining regions
CE-SDS-NGS	capillary electrophoresis sodium dodecyl sulfate-non gel sieving
ESI-TOF-MS	electrospray time-of-flight mass spectrometry
FTIR	Fourier transform infrared
HBS-EP buffer	hEPES-buffered saline EDTA polysorbate buffer
HC	heavy chain
HIC	hydrophobic interaction chromatography
HUVEC	human umbilical vein endothelial cell
IEC	ion exchange chromatography
LC	light chain
MAb	monoclonal antibody
SDS	sodium dodecyl sulfate
SEC-MALLS	size exclusion chromatography with multi angle laser light scattering
SPR	surface plasmon resonance
TEM	transmission electron microscopy

Electronic supplementary material The online version of this article (doi:10.1007/s11095-012-0732-6) contains supplementary material, which is available to authorized users.

R. Paul • H. Beck • A. Briguet • V. Schnaible • T. Buckel • S. Boeckle (✉)
Pharma Technical Development Europe (Biologics) Analytics
F. Hoffmann-La Roche Ltd.
4070 Basel, Switzerland
e-mail: sabine.boeckle@roche.com

A. Graff-Meyer • H. Stahlberg
Center for Cellular Imaging and NanoAnalytics (C-CINA), Biozentrum
University of Basel
Basel 4085, Switzerland

M. E. Lauer • A. C. Rufer
Discovery Technologies, F. Hoffmann-La Roche Ltd.
Basel 4070, Switzerland

INTRODUCTION

Protein aggregation in therapeutic biotech products is still one of the 'hot topics' discussed in the field of biopharmaceutical development, toxicology, immunology and clinical pharmacy. Since protein aggregates potentially impact drug performance (potency, pharmacokinetic, pharmacodynamics) and safety (immunogenicity, adverse effects) (1–3) the level of aggregates in biopharmaceuticals has to be closely monitored as a critical quality attribute. As the different methodologies that are routinely used for the determination and characterization of aggregates have their own strengths and weaknesses (4–9) little is known about the detailed structure of such aggregate species, and as a consequence about their potential effect on biological function and safety. In addition, it often remains unclear whether there are 'good' and 'bad' protein aggregates, and knowledge about the pathway of protein aggregation or knowledge about the mechanisms that control the aggregation process is limited (10–13). With regard to immunogenicity, animal models have clearly demonstrated that protein aggregates of degraded samples enhance the immune response (14–16). However, the applied samples were mostly containing large amounts of various aggregates which were rather little characterized and therefore it is currently not clear which specific types and doses of aggregates may induce an effect. In order to better understand the biological effect of protein aggregates in biopharmaceutical drug products, a thorough characterization of such species is a prerequisite. There have been many studies focusing on the characterization of antibody aggregates. For example, the formation of antibody aggregates has been studied after agitation stress, shaking, freeze thaw, pH or light stress (8,17–20). However, these stressed antibody solutions were containing a mixture of various aggregate species besides residual monomers. In order to allow detailed structural characterization of a certain type of aggregates, isolation and purification of aggregate species is required. Samples containing an enriched amount of antibody dimers have been studied by Remmele *et al.* (21) and three predominantly covalent dimeric forms in their isolated dimer pool were detected.

The purpose of this study was to prepare highly purified monoclonal antibody dimer species from differently stressed bulk solutions of one monoclonal IgG1 antibody in order to enable a thorough characterization of the molecular architecture and function of dimer species and to understand the impact of the applied pharmaceutical relevant stress conditions on the formation of dimer forms. A model IgG1-antibody was therefore stressed under three different stress conditions which were related to conditions that an antibody molecule may experience during processing or during storage. First, process-related stress was applied as a 'realistic' stress condition as this stress included all typical steps of upstream and downstream processing which are performed during manufacturing of monoclonal antibodies. To enforce the stress onto the antibody molecules, accelerated stress conditions were also applied. Stress attributed to pH shifts is known to potentially induce aggregation, e.g. during freeze/thaw procedures of bulk or during the virus inactivation step in purification (22,23). Therefore, the pH of a model IgG1 solution was titrated down to pH 2.5 and then back to pH 6.2 to induce aggregation. Finally, intensive light stress by exposure to UV-light, which can induce chemical denaturation and aggregation (24), was applied to induce aggregate formation in the model antibody solution. The respective antibody dimer species which were generated due to the three different stress conditions were afterwards isolated and purified to enable thorough structural characterization with regard to their biophysical, biochemical and three dimensional structures in comparison to the monomeric antibody molecule. *In vitro* functional assays and a cell based potency assay were finally used to study the impact of structural modifications on binding affinity and biological activity.

MATERIALS AND METHODS

Materials

An IgG1 monoclonal antibody (MAb) was chosen as a model antibody for the present study. For the isolation of process stress dimers and monomer 6 g antibody bulk solution obtained from a large scale manufacturing campaign after the virus inactivation step was used. This bulk material was in a buffer consisting of 90 mM Acetic acid, 110 mM Tris, and 20 mM Citric acid, pH 5.5. For pH and light-induced stress, approximately 4 g of formulated antibody solution (25 mg/ml, pH 6.2) in a buffer containing 51 mM Sodium Phosphate, 6 % Trehalose, and 0.04 % Polysorbate 20 was used as starting material.

Stress Conditions

For pH stress, 150 mM ortho-phosphoric acid was added drop-wise to a volume of 150 ml of formulated antibody solution while slowly stirring. When the solution reached a pH of 2.5, the solution was incubated at room temperature for 1 h (without stirring). Afterwards, the solution was titrated back to pH 6.2 with 150 mM Na_2HPO_4, resulting in an increased total volume of approx. 280 ml with a determined protein content of 15.0 mg/ml. Light-induced stress of formulated antibody solution was performed using the SunTest XLS + device. Ten glass vials containing 16 ml of antibody solution were kept under the UV–VIS light (Irradiance Energy 765 W/m^2) for 20 h. The bulk solutions of all stressed solutions were stored at −80 °C after stressing.

Purification of Antibody Monomer and Dimers

For the purification and isolation of monomer and dimer fractions the frozen bulk samples were thawed at 25 °C in a water bath and filtered through 0.2 µm pore-size filters to remove any precipitates. Preparative ion exchange chromatography (IEC) was performed using a Poros 50 HS column (column volume 470 ml) at a flow-rate of 65 ml/min using gradient-elution with buffer A (35 mM Na-Acetate; pH 5.5) and buffer B (35 mM Na-Acetate / 500 mM NaCl; pH 5.5). The stressed bulk antibody samples were loaded undiluted onto the column and fractionation was performed based on UV detection at 280 nm. The separated fractions were analyzed by SE-HPLC similar as described for SEC-MALLS. The monomer fraction (isolated out of the process stress bulk) and dimer fractions from the cation-exchange step were pooled and concentrated by centrifugation using 50 ml Amicon ultracentrifuge filter units (MWCO of 30 kDa, 4000 rpm) resulting in a final volume of approx. 12 ml. The monomer fraction was dialyzed using tangential flow filtration method resulting in a final buffer medium of 51 mM Sodium Phosphate. The concentrated dimer fractions were further purified using a Superdex 200 preparative SEC column with 320 ml column volume and 600 mg sample load capacity at a flow rate of 2.5 ml/min. Sodium phosphate buffer (51 mM, pH 6.2) was used as elution buffer. The final monomer and dimer fractions in 51 mM phosphate were sterile filtered and frozen in aliquots at −80 °C. The isolated monomer fraction out of the process stress bulk was used as monomeric antibody in this study. The protein content in the fractions was determined by measuring the absorption at 280 nm using a UV–VIS spectrophotometer Lambda 35 (Perkin Elmer).

Size Exclusion Chromatography with Multi-angle Laser Light Scattering (SEC-MALLS)

For SEC-MALLS analysis, volumes of 10 µl to 60 µl of undiluted antibody samples (corresponding to 30 µg for dimers and 50 µg for monomers) were applied onto a TosoHaas TSK-Gel G3000SWXL column and separation was performed with 0.2 M K_2HPO_4, 0.25 M KCl, pH 7.0 at a flow rate of 0.5 ml/min for 30 min. Molecular weight determination was performed using a MiniDawn TREOS light scattering detector (Wyatt Technology, Germany) and the Astra V Software Version 5.3.4.14 (Wyatt Technology, Germany). Molecular weight determination was calibrated by a single injection of BSA. The acceptance criterion for the calculated molecular weight of BSA monomer was 66 kDa (+/− 10 %).

Analytical Ultracentrifugation (AUC)

Sedimentation velocity experiments were performed on a Beckman Coulter XLI instrument with an An50Ti rotor and Spin Analytical Spin60 centerpieces. Samples were diluted to 0.5 mg/ml in sample buffer (51 mM sodium phosphate pH 6.2) and were centrifuged at 42,000 rpm /20 °C. Sedimentation profiles measured in triplicates at 280 nm were analyzed with Sedfit/Sedphat (25). First, sedimentation coefficient distributions c(s) were calculated for the individual samples in Sedfit. Then, using a "hybrid global continuous distribution and global discrete species" model in Sedphat, global fits to the triplicate data for each of the monomer and dimer species were calculated. Sedphat reports sedimentation coefficients corrected for buffer density and viscosity ($s_{20,w}$) and corresponding signal-weighted sw20,s values for integrations of peaks. Relative species abundance (area %) were calculated by integration of the sedimentation coefficient distributions $c(s_{20,w})$ in Origin (vers. 7.5 SR7). The frictional coefficient f/f_0 is the effective frictional coefficient of a particle divided by the frictional coefficient of a sphere with identical molecular weight and is thus a measure of shape. A partial specific volume of 0.726 g/ml was used for all antibody samples. For analysis of the light stress and pH stress dimers two sedimentation coefficient ranges were used in Sedphat: one accounting for the residual monomer in these samples (frictional coefficient fixed to that calculated for the monomer sample) and the other segment describing the sedimentation coefficient distribution of the dimers and traces of higher oligomers.

Peptide Mapping

Prior to digestion, samples were denatured in 0.4 M Tris-buffer, pH 7.5, containing 8 M Guanidine-hydrochloride. Trypsin digestion was performed by incubation at 37 °C for 20 h in a digestion buffer (0.1 M Tris/HCl, 1 mM $CaCl_2$, pH 7.5) containing trypsin (modified by reductive methylation) in a trypsin to MAb ratio of 1/20 (*w*/*w*) of the protein by weight. Digestion was stopped by adding a 1 % TFA solution. For chromatographic separation a Capillary-LC system (Agilent 1100 Series Capillary LC System) was used with a RP-C18 Phenomenex Jupiter column (250×0.5 mm, 5 µm, 300 Å) with a gradient of water / 0.1 % formic acid to acetonitrile / 0.1 % formic acid at a flow rate of 20 µl/min. Subsequent analysis of chromatographic peaks observed at 220 nm was done by electrospray time-of-flight mass spectrometry (ESI-TOF-MS) in the positive ion mode on a Waters Q-Tof Ultima, achieving sequence coverage of greater than 95 %.

Capillary Electrophoresis Sodium Dodecylsulfate-Non-Gel Sieving (CE-SDS-NGS)

CE-SDS-NGS was performed both under reducing, and non-reducing conditions. Samples were treated with SDS (and

Dithiothreitol for reducing conditions) for 5 min at 70 °C before injection in a Beckman Coulter Capillary Electrophoresis System ProteomeLabPA800. The capillary was rinsed at 70 psi with 0.1 mM NaOH for 5 min and then with 0.1 mM HCl and deionized water for 1.0 min. The SDS-MW Gel Buffer was loaded into the capillary at 50 psi for 15 min from the outlet side. Samples were injected electrokinetically at 10 kV for 10 s. Analysis was performed in the negative polarity mode (−15 kV, −480 V/cm). Maintaining the capillary temperature at 40 °C, a typically obtained current value was 35–40 μA.

Fourier Transform Infrared (FTIR) Spectroscopy

Infrared spectra were acquired using a Thermo Scientific (Thermo Electron Corporation, USA) Nicolet 6700 Fourier transform infrared spectrometer. Samples were loaded into a flow-cell (Smart Proteous sample compartment) with CaF_2 windows with a 6 μm fixed pathlength well. A 128-scan interferogram was collected for each spectrum in single beam mode with a 4 cm^{-1} resolution. Protein concentration was approx. 10 mg/ml for all the samples subjected to FTIR analysis. A buffer blank spectrum was used as the background before each sample measurement. Protein absorbance spectra were obtained by subtraction of the buffer blank from the protein spectrum. Water vapor signals, if present, were removed by subtracting the spectrum of gaseous water. Data were analyzed with the OMNIC™ software tool and displayed as second derivative amide I spectra with a 9-point smoothing.

Papain Digestion Combined with IEC and ESI-TOF-MS Analysis

Samples were incubated with papain at an enzyme substrate ratio of 1/100 in 50 mM sodium phosphate buffer, pH 7.4 in the presence of 1 mM cysteine and 4 mM EDTA at 25 °C for one hour. After digestion, buffer exchange into 20 mM sodium phosphate buffer, pH 6.0 was performed using PD Minitrap columns (GE Healthcare, Switzerland). Samples were stored on ice before separation by cation exchange HPLC. Samples were separated on a Dionex ProPac WCX-10 column (4×250 mm) on a Waters Alliance 2695 separation module with UV detection at 280 nm using a linear gradient of eluent buffer A (20 mM sodium phosphate, pH 6.0) and buffer B (0.5 M sodium chloride in 20 mM sodium phosphate, pH 6.0) at a flow rate of 1.0 ml/min (2 % to 39 % B within 21 min). The main peaks in the chromatogram were then fractionated using an automatic fraction collector and concentrated over 10 kDa membrane filters (Sartorius, Vivaspin 6). The peaks were characterized by ESI-TOF-MS using an Agilent 1100 chromatography system with a Poroshell SB-C8 column (Agilent, 75 x 0.5 mm, 5 μm, 300 Å). Mobile phases were water / 0.1 % formic acid and acetonitrile / 0.1 % formic acid. Total runtime was 30 min with a linear gradient from 20 % B to 95 % B within 10 min and a flow rate of 15 μl/min. Subsequent analysis of chromatographic peaks was carried out using a Waters Q-TOF mass spectrometer, equipped with an electrospray source (ESI) in the positive ionization mode. The capillary voltage was set to 3 kV, the cone at 50 V, the source temperature at 80 °C, the desolvation temperature at 250 °C with a gas flow of 350 L/h. Exact mass was calculated using a MaxEnt1 spectra deconvolution.

Transmission Electron Microscopy (TEM)

For TEM experiments, the antibody stock solutions were diluted to 10 and 5 μg/ml with PBS buffer. 4 μl of diluted samples were adsorbed for 60 s to glow-discharged parlodion carbon-coated copper grids. The grids were then blotted, washed on five drops of double-distilled water and negatively stained on two droplets of 2 % uranyl acetate (pH 4.3) solution. Tobacco Mosaic Virus (TMV) was introduced as a size calibration standard and for staining quality evaluations (26). Samples were imaged at a nominal magnification of 130000X using a Philips CM10 electron microscope (Philips, Eindhoven, The Netherlands) operating at 80 kV. Electron micrographs were recorded on a 2000 by 2000 pixel charge-coupled device camera (Veleta, Olympus soft imaging solutions GmbH, Münster, Germany) mounted in the 35 mm port of the TEM, yielding a final pixel size of 0.36 nm on the specimen level. Reference-free alignment was performed on manually selected particles from recorded image using the EMAN image processing package (27). A total of 500 particles of each imaged samples (monomers or dimers) were extracted from the micrographs, aligned, and classified by multivariate statistical analysis to calculate class averages. The class averages with the best signal-to-noise ratio were presented in Fig. 7.

Potency Assay

The Human Umbilical Vein Endothelial Cell (HUVEC) anti-proliferation bioassay is based upon the ability of the antibody to inhibit antigen-induced HUVEC proliferation by preventing the antigen from binding to the receptor for antigen on HUVEC cells. The assay is performed in 96-well tissue culture microtiter plates. Varying concentrations of antibody reference material or samples are mixed with antigen (60 ng/ml) and incubated for 30–90 min at ambient temperature. 50 μL of the antigen/antibody mixtures are then added to the microtiter plates, followed by the addition of 50 μL of HUVEC suspension (10,000 cells/well). The plates are incubated at 37 °C, 5 % CO_2 in a humidified incubator for 4 days, after which 25 μL of the redox dye

AlamarBlue is added. The plates are then incubated for 6 to 7 h at 37 °C, 5 % CO_2 in a humidified incubator, and the relative number of viable cells is quantified indirectly by reading the fluorescence using a 96-well fluorometer with excitation at 530 nm and emission at 590 nm. AlamarBlue is blue and non-fluorescent in its oxidized state, but is reduced by the intracellular environment into a pink form, which is highly fluorescent. The changes in color and fluorescence are proportional to the number of viable cells. The results, expressed in relative fluorescence units (RFU), are plotted against antibody concentrations, and a parallel line analysis is used to estimate the inhibitory activity of samples relative to native monomer as reference material. Inhibition of HUVEC proliferation is proportional to the antibody concentration (specific biological activity). Each sample is measured in triplicate (precision of the assay is 4–6 % RSD). Note that for the process stress and light stress dimers the concentration range of the assay had to be adapted and the potency of these samples relative to the native monomer was determined using a 4-parameter fit of the dose–response curves and EC50 ratios.

FcγRIIIa-Binding Analysis by Surface Plasmon Resonance (SPR)

The ability of IgG1 in monomer and dimer samples to bind FcγRIIIa[Val-158] was examined by SPR measurement using a BIAcore 3000 system (BIACORE, Uppsala, Sweden). Anti-GST antibody (GST Capture Kit, Biacore) was immobilized on a carboxymethylated dextran sensor (CM5 chip, BIACORE) using an amine coupling kit (BIACORE). In the same way, anti-hGCSF antibody was immobilized on the sensor chip to produce a reference surface. Soluble recombinant human FcγRIIIa[Val-158] carrying a GST tag, produced in HEK293 cells was captured by the immobilized anti-GST antibody by injecting the soluble GST-FcγRIIIa until a response level of about 30 RU were reached. Samples were diluted to mass concentrations corresponding to monomer concentrations of 12 nM and 8750 nM in HBS-EP buffer (0.01 M HEPES, 0.15 M NaCl, 3 mM EDTA, 0.005 % polysorbate 20, pH 7.4) and each diluted sample was injected at a flow rate of 30 µL, using HBS-EP as running buffer. Monomer sample was measured in duplicate (16 % RSD). Regeneration of the chip was performed by injection of 40 mM HCl for 1 min at a flow rate of 30 µL/min. The obtained data were corrected for the blank control and molar concentrations were calculated using SEC-MALLS data prior to analysis with various kinetic models and fitting methods using BIACORE 4.1 kinetic evaluation software. For comparison of the different samples, relative binding affinities were calculated from steady-state data (equilibrium binding constants) normalized to the monomer sample.

RESULTS

Isolation and Chromatographic Characterization of Dimer Species

Soluble antibody dimers from solutions that experienced three different stress conditions were isolated in a two-step procedure using preparative cation exchange chromatography and size exclusion chromatography (SEC). According to analytical SEC, the content of dimer species in the bulk solutions after initial stress was approx. 4 area% for process stress, 7 area% for pH stress and 20 area% for light stress. Characterization of the isolated fractions by analytical SEC-MALLS resulted in SEC profiles showing main peaks at the retention time typical for dimer species for all fractions with 88 area% for process stress, 81 area% for pH stress, and 67 area% for light stress induced dimers (Fig. 1 and Table I). The isolated and purified dimer species were not dissociable by dilution in low ionic strength phosphate buffer or in SEC mobile phase with a high ionic strength. It should be noted that dissociable dimers potentially present directly after stress were most likely lost during the purification process. The determined molecular weight of approximately 300 kDa for all three dimer peaks in the isolated fractions corresponds to the theoretically expected molecular weight of IgG1 dimers. The respective peak maxima in SEC of the three dimers were, however, found at slightly different retention times (Fig. 1), indicating that the stress conditions led to dimer species with different hydrodynamic diameters. According to the retention times of the peak maxima, the hydrodynamic diameter was highest for process stress dimers, medium for light stress dimers and smallest for pH stress dimers.

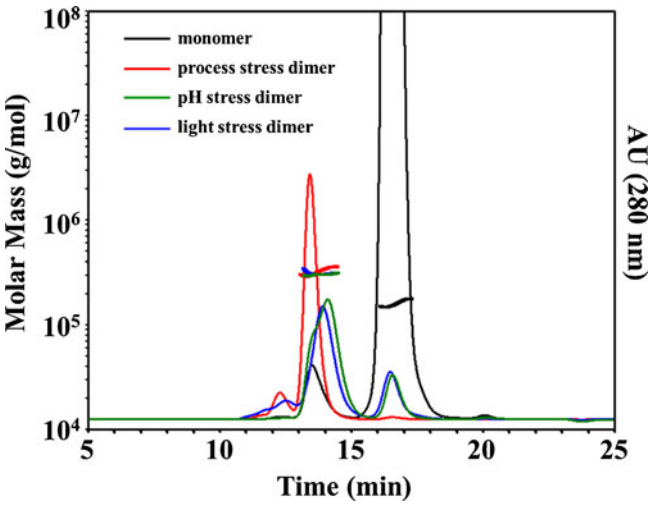

Fig. 1 SEC-MALLS chromatograms of monomer and stress induced dimers The chromatograms represent relative absorbance at 280 nm, and the lines (at each major peak position) represent the molecular weight distribution in g/mol.

Table I Composition of Purified Monomer and Stress Induced Dimers According to SEC

Sample	Area % monomer	Area % dimer	Area % oligomers
Monomer	98	2	0.1
Process stress dimer	1	88	10
pH stress dimer	17	81	1
Light stress dimer	22	67	13

Analytical ultracentrifugation (AUC) performed with samples diluted in sample buffer (51 mM sodium phosphate) to a concentration of 0.5 mg/ml confirmed the percentage of dimer species in all three fractions determined by SEC (Fig. 2). Sedimentation coefficients determined by AUC increased in the order process stress dimer < light stress dimer < pH stress dimer, while the frictional coefficients decreased in this order (Fig. 2). Since all dimers had the same molecular weight, the frictional coefficients were a direct measure of the relative shape of the dimers: process stress dimers were most extended in solution, while pH stress dimers were the most compact dimer species and light stress dimers showed an intermediate compactness.

Furthermore, characterization of the different dimer fractions by analytical hydrophobic interaction chromatography (HIC) and ion exchange chromatography (IEC) showed significant differences between the samples in terms of hydrophobic behavior and charge profile. Whereas process and pH stress dimers displayed distinct dimer peaks in IEC, a broad distribution of peaks was found for light induced dimers. The HIC profile for light induced dimers was also very broad,

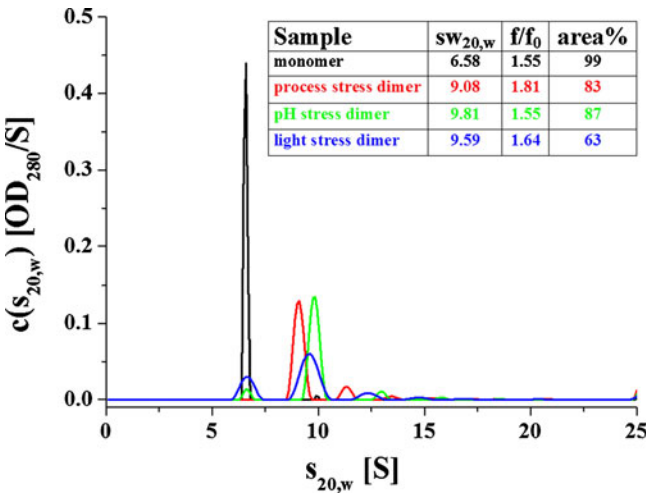

Fig. 2 Sedimentation coefficient distributions of monomer and stress induced dimers analyzed by AUC. The x-axis shows the sedimentation coefficient corrected for buffer viscosity and density at 20 °C; the y-axis shows the relative abundance of the species in signal units per sedimentation coefficient. The area% refer to the main peaks: monomer peak for the native monomer sample and dimer peaks for the stress induced dimers.

indicating the presence of several different dimer species in the light stress dimer fraction. According to the HIC chromatograms, the pH stress dimers appeared to be more hydrophobic than the process stress dimers because the resulting peaks accounting for the pH stress dimer were obtained at higher retention times than for the process stress dimer (Supplementary Material Figure S1).

Assessment of Chemical Modifications in Dimer Species

To assess potential chemical modifications induced by the applied stress conditions, characterization by LC/MS-peptide mapping was performed with all three dimer fractions and compared to the unstressed monomeric antibody. The LC/MS-peptide map chromatograms of process stress dimers and pH stress dimers showed no differences compared to the chromatogram of the monomer (data not shown). In contrast, light stress dimers showed significant differences in the peak pattern compared to the monomer, which could be mainly attributed to oxidation of methionine residues (Fig. 3 and Supplementary Material Table SI). Besides Met oxidation, some other chemical modifications were determined in the light stress dimer, which could not be further identified ("unknown peaks" in Fig. 3). In addition, a number of peaks showed different intensities, however, the same peptides were identified by MS data for both monomer and light stress dimers.

For further evaluation of chemical modifications, CE-SDS-NGS was separately performed under reduced and non-reduced conditions. Under both conditions, the process stress dimers showed the same peak pattern in the electropherogram as the monomer, indicating full dissociation of process stress dimers by SDS treatment (Fig. 4). Under non-reduced conditions, the pH stress dimer fraction showed one major peak at the monomer position (80 % CPA) together with a second peak of 20 % CPA in the aggregate region (data not shown). Under reducing conditions using SDS-

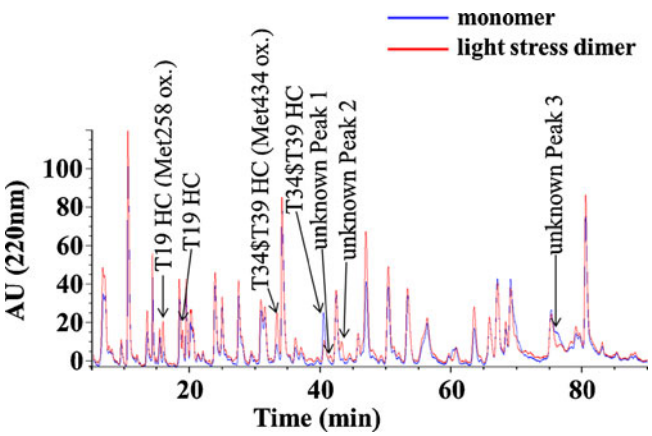

Fig. 3 LC/MS-peptide map chromatograms at 220nnm of light induced stress dimer in comparison to monomer.

buffer and DTT, the majority of the pH stress dimer was cleaved to light chain (LC) and heavy chain (HC) fragments (Fig. 4). In contrast, the light stress dimers showed clear peaks in the aggregate region of the electropherogram both under reduced (Fig. 4) and non-reduced conditions. SDS-buffer treatment alone only led to dissociation of 34 % of dimers into monomer molecules and 52 % remained as aggregates. Under reduced conditions, SDS and DTT treatment dissociated approx. 70 % of the light stress dimers into LC and HC and approx. 30 % were still detected in the aggregate region.

Structural Assessment of Dimer Species

Changes in the secondary structure of protein aggregates can be detected by Fourier Transform Infrared (FTIR) Spectroscopy (19,28,29). Interestingly, the antibody dimers isolated after different stress conditions did not show any difference by visual comparison in their second derivative spectra in comparison to the monomer (Fig. 5), suggesting no major alteration of the secondary structure of dimers. The β-sheet content of the dimers and the monomer was determined to be around 45 % in all samples.

In order to evaluate at which site the antibody monomers are associated with each other to build the different dimer molecules, papain digestion was performed followed by IEC, in an analogous way as described by Lau *et al.* (30). In addition, peaks after IEC were fractionated and analyzed by both MS and SEC-MALLS for identification of the species. In comparison to the digested monomer showing two peaks for the Fc (at approx. 9 min) and Fab fragment (at 12 min), respectively, one additional peak (at 15.5 min) was obtained with the papain digested process stress dimer (Fig. 6a). This third peak was composed of Fab parts as demonstrated by MS and, according to SEC-MALLS, had a molecular weight of approx. 100 kDa, which corresponds to a Fab-dimer. The additional

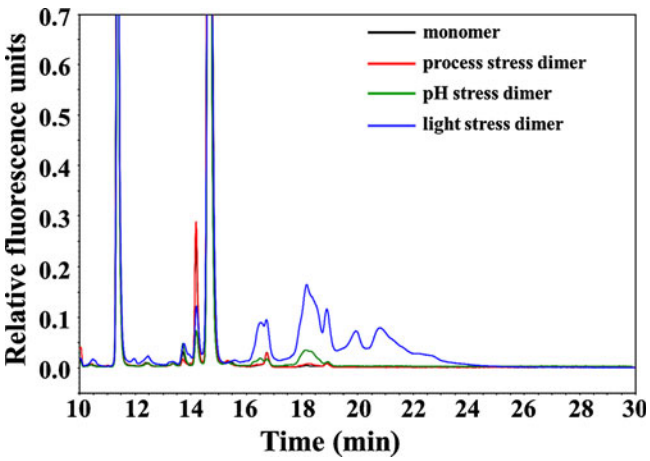

Fig. 4 CE-SDS-NGS electropherograms under reduced conditions of monomer and stress induced dimers.

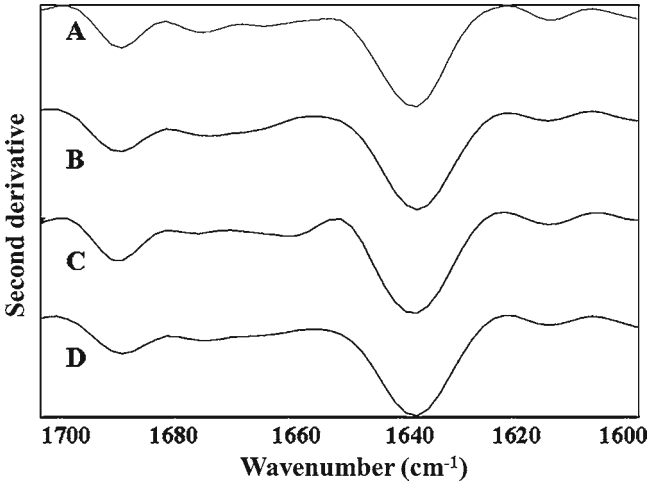

Fig. 5 FTIR second derivative spectra of (*A*) monomer and stress induced dimers (*B*: pH stress dimer; *C*: process stress dimer; *D*: light stress dimer).

peak was also observed for the pH stress dimer (Fig. 6b) but with lower intensity compared to the free Fab fragment. Moreover, the intensity of the Fc fragment was reduced for pH stress dimers. For the light stress dimer the identity of the peak at the position of the Fab fragment was confirmed by MS as Fab fragment. No other distinct species could be identified in the broad distribution of signals in the IEC (Fig. 6b).

To acquire further structural information on individual antibody dimers, such as conformations and sizes, the different antibody dimer samples were imaged by negative-stain transmission electron microscopy (TEM) and submitted to class averaging using single-particle analysis of TEM electron micrographs. The antibody monomer sample was used as a

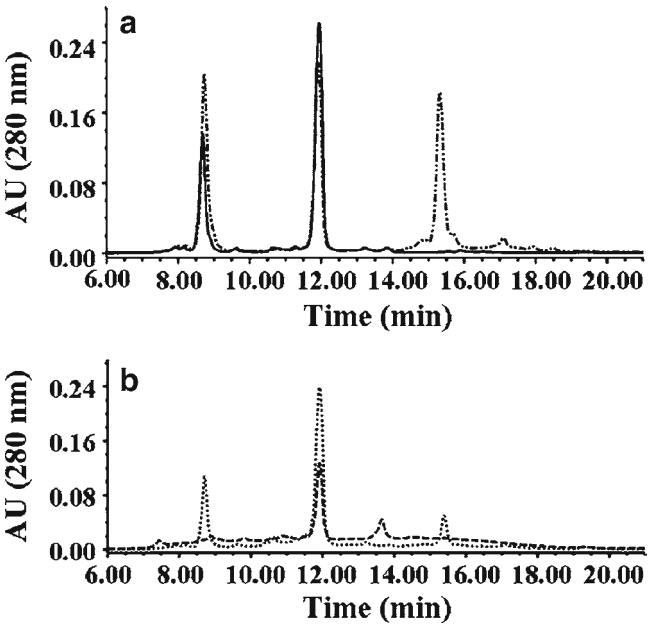

Fig. 6 IE-HPLC chromatograms at 280 nm of (**a**) papain-digested monomer (black line) and process stress dimer (dotted line) and (**b**) pH stress dimer (dotted line) and light stress dimer (dashed line).

control. Length and shape of the antibody monomer shown in the class average image (Fig. 7a, inset) were in accordance with the known structure of an IgG1 molecule (31–33). The sample preparation did not lead to any nonspecific monomer aggregation. The average projections calculated by single particle analysis of the different antibody dimer images are uniformly different as shown in Fig. 7. The TEM electron micrographs and the class averages of process stress dimers (Fig. 7b) show dimer molecules, where two monomer molecules are attached to each other via one distinct domain. This particular dimer conformation was termed the 'bone-like' structure with an end-to-end distance of 28.9 nm. Both monomers involved in the process stress dimer association show three intact domains and the overall typical Y-shape. The TEM electron micrographs and a class average image of pH stress dimers (Fig. 7c and inset) show a dimer conformation where the monomer molecules are associated via two domains. This conformation is more compact and was termed the 'close' conformation. The distance between the two terminal domains of the pH stress dimer is shorter (25.9 nm) compared to the distance of process stress dimer (28.9 nm). In contrast to the process and pH stress dimers, the light stress dimers showed a variety of different dimer conformations, one example of a class-average image is shown in Fig. 7d (inset). Some light stress dimers present a 'bone-like' conformation as observed in the process stress dimer images, but also a 'bended bone' conformation together with a 'close' conformation, as observed in case of pH stress dimers. Furthermore, new dimer conformations were identified, such as orientation of two antibody molecules like a sandwich. For some light stress dimers no clear orientation could be described. The average end-to-end distance of the light stress dimers is 26.2 nm, which lies between the end-to-end distance of the process stress dimer and the pH stress dimer.

Finally, it is important to note that for all dimer species, the overall antibody Y-shape still remained intact and could clearly be identified by negative stain TEM imaging.

Functional Characterization of Dimer Species

In order to gain further insight into the structure and functionality of the three different antibody dimers with regard to their binding affinity towards antigen and accessibility of the Fc region, a cell based potency assay and binding experiments using surface plasmon resonance (SPR) were performed with the respective dimer fractions.

For the determination of the bioactivity of the different dimers in comparison to the monomeric antibody a specific anti-proliferation bioassay was used. The assay set-up monitors the binding affinity of the Fab domains of antibodies towards their antigen. The results are summarized in Table II and Fig. 8. The process stress dimer displayed a

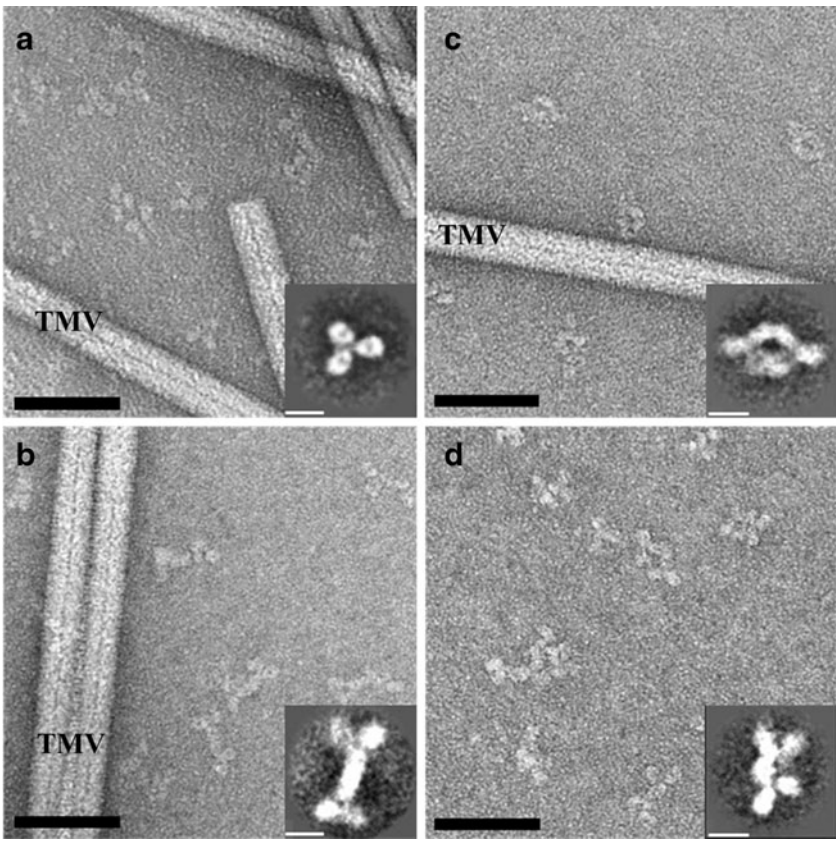

Fig. 7 Negative stain transmission electron microscopic images of (**a**) monomer, (**b**) process stress dimer, (**c**) pH stress dimer and (**d**) light stress dimer. The scale bar, shown in black line represents 50 nm. The insets show class average images of monomer (**a**) and respective dimers (**b**, **c**, **d**). The white scale bar in each inset represents 10 nm. Tobacco Mosaic Virus (TMV) was used for size calibration and evaluation of staining quality.

significantly reduced bioactivity of 62 % (RSD 3 %) compared to the monomer. The pH stress dimer showed a biological activity similar to the monomer (101 % rel. potency, RSD 4 %). The light stress dimer displayed a significantly reduced potency compared to the monomer (21 % rel. potency, RSD 17 %). It has to be noted that the slope of the dose–response curve was reduced for the light stress dimer in comparison to the monomer. Therefore, the biological response cannot be regarded as similar and the calculated relative potency value for the light stress dimer has to be considered as approximation. Western Blot analysis moreover revealed that light stress dimers were not able to bind antigen, whereas the residual amount of monomeric molecules present in this particular dimer fraction were binding antigen (data not shown).

The accessibility of the Fc region within the different dimer species was investigated by measuring the binding characteristics to the receptor FcγRIIIa [Val-158] by surface plasmon resonance using the BIAcore biosensor system. For all dimer fractions, the dissociation rates were decreased compared to the monomer resulting in a 3-5-fold higher overall relative binding affinity to FcγRIIIa (Table III), indicating the involvement of a second binding site per molecule. The binding kinetics obtained with the process stress dimer can be described by a two-state model (Fig. 9), while the pH stress and light stress dimer showed complex kinetics (data not shown).

DISCUSSION

In the present study an IgG1 monoclonal antibody was exposed to different stress conditions to induce the formation of aggregates: process stress, pH stress and light stress. From the resultant aggregates, the species accounted for soluble antibody dimers were isolated and purified to obtain enriched dimer fractions with a purity of 67–88 % based on area % of SEC. A systematic combination of complementary methods to assess biochemical, structural and biological features of the antibody dimers allowed detecting structural differences within the dimers and in comparison to the monomer. The impact of these structural modifications on the binding affinity and bioactivity of the dimers was evaluated. Based on the conclusions we were able to propose a schematic model of the three different dimer conformations including their capacity to bind antigen (Fig. 10).

Table II Relative Potencies of Stress Induced Dimers Determined by a Cell-Based Bioassay

Sample	Mean relative potency	RSD (%)
Process stress dimer	62	3
pH stress dimer	101	4
Light stress dimer	21[a]	17

[a] Biological response was not similar

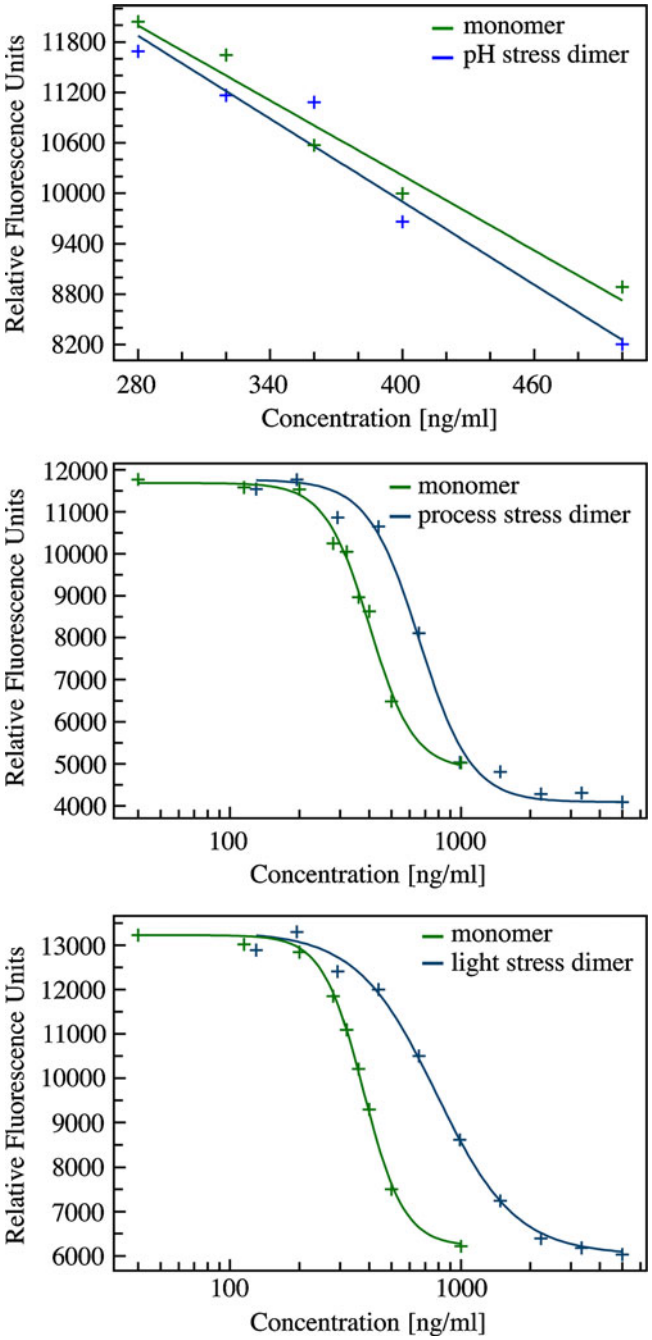

Fig. 8 Dose–response curves of stress induced dimers (blue lines) relative to the monomer (green lines) determined by a cell-based bioassay. Parallel line analysis was used to determine relative potency of pH stress dimers; a 4-parameter fit of the dose–response curves and EC50 ratios were used to determine relative potencies for process stress and light stress dimers.

Characterization of Process Stress Dimers

Process stress dimers (Fig. 10a) that were generated during the standard antibody manufacturing process exposed a

Table III Relative Binding Affinities to FcγRIIIa by SPR

Sample	Rel. affinity (%)
Monomer	100 (16 % RSD)
Process stress dimer	430
pH stress dimer	460
Light stress dimer	310

fully native primary structure according to MS and CE-SDS-NGS analysis. Electron microscopy has been previously used to characterize the structure of e.g. immune complexes of polyclonal IgG solutions or also to image IgG aggregate mixtures, demonstrating the suitability of TEM or STEM for the characterization of antibody aggregates (32,34–36). In this study, high resolution negatively stained TEM was performed using purified dimer species and this enabled to obtain information of the dimer's molecular structures and architectures. A 'bone like' structure was observed by TEM imaging where two antibody molecules were attached to each other via one distinct domain (Fig. 7b). Because of the symmetrical 'tripod' configuration of each individual IgG monomer and the flattening effect of the carbon surface on the IgG molecules it was not possible by TEM analysis alone to clearly differentiate which part of the molecule (Fab or Fc) was involved in the formation of the bone-like dimer. Characterization of peptide fragments after papain digestion revealed that the process stress dimers were formed via the association of one Fab domain of each antibody molecule (Fig. 6a). Dimerization via the Fab domain is likely a common attribute for antibodies as this was for example also proposed as potential mechanism for the observed self-association or aggregation effects of other studied IgGs (30,37,38). Although process stress dimers were only associated via this single interaction site at the end of the Fab domain, these dimer species were stable in salt buffers (e.g. during SEC, IEC or HIC analysis) or upon dilution in sample buffer. The dimer bond in process stress dimers was, however, readily dissociated by SDS. Therefore, hydrophobic interactions between the two

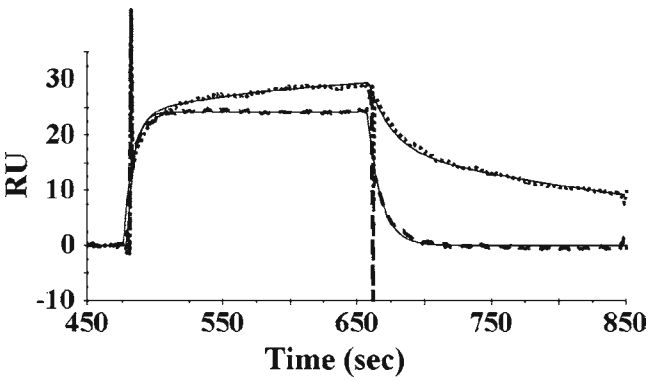

Fig. 9 Surface plasmon resonance analysis of FcγRIIIa binding of the monomer (dashed line) and process stress dimer (dotted line). The thin black lines show the applied mathematical fits.

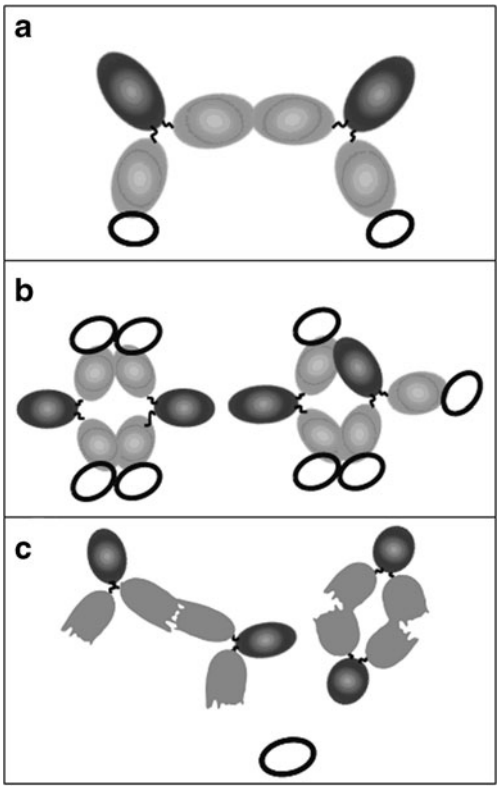

Fig. 10 Schematic representations of the proposed dimer conformations and their ability to bind antigen. (**a**) process stress dimer; (**b**) pH stress dimer and (**c**) light stress dimer. The Fab domain of the antibody is shown in grey and the Fc domain in black. The antigen is represented by the oval-shaped open circles.

Fab molecules obviously play an important role in stabilizing the dimer. Besides the single intermolecular interaction site to form the dimer, no other structural differences were determined between the process stress dimer and the native antibody monomer with regard to their secondary structure (FTIR), tertiary or quaternary structure (TEM). The process stress dimers exposed a high similarity in their bone-like conformations according to TEM and this was also reflected by IEC and HIC results showing that species were homogeneous with regard to their exposed surface charges and hydrophobicity. The 'bone-like' dimer structure had a strong impact on the binding affinity towards antigen and the resulting bioactivity: the Fab-Fab interaction within the dimer molecule led to reduced antigen binding and reduced potency (Table II, Fig. 8) most likely due to partial blockage of the CDR region. Because of the stretched bone-like conformation, the overall hydrodynamic diameter of the process stress dimer type is rather large which explains the relatively short retention time in SEC (Fig. 1) as well as the lower sedimentation coefficient and higher frictional coefficient in AUC (Fig. 2) compared to the other dimer species. Therefore, the process stress dimer clearly exposed the most extended shape compared to the other dimer species, both in solution and on the carbon surface of the TEM grid. Whereas the Fab domain was partially impaired

due to the dimerization the Fc domain appeared to be fully native in the process stress dimers. SPR allows assessing the dimers' ability to bind to the receptor FcγRIIIa at the Fc part of the hinge region, close to the glycosylation site at the proximal end of CH_2 domain. Binding of the Fc part of IgG1 to the FcγRIII receptors on effector cells is a critical part of the Antibody-Dependent Cellular Cytotoxicity (ADCC) and is therefore an important attribute for the Fc function of some specific therapeutic monoclonal antibodies (39,40). The good applicability of the two-state model on the binding kinetics of process stress dimers (Fig. 9) indicates a homogenous composition of dimer species with both Fc domains accessible and active for binding to FcγRIIIa. Because of the two active binding sites at both ends of the 'bone-like' dimer the overall binding affinity is increased compared to the monomer (Table III).

Characterization of pH Stress Dimers

The pH stress dimers were generated by incubation of the antibody solution at a low pH of 2.5 for 1 h followed by back-titration to a pH of 6.2. It was reported that exposure of antibodies to a low pH can affect stability of the protein structure and induce aggregation (22,41,42) and that this may be because of destabilization and unfolding of the CH_2 domains of the Fc part (43) or alternatively because of unfolding of the Fab domain and CH3 domain as reported by Brummitt *et al.* (44). However, besides exposure to a low pH of 2, also the process of neutralization may be the reason why aggregates were obtained after pH stress (22). According to the MS results, the performed pH cycle had no impact on the primary structure of the antibody. The antibody dimers induced by pH stress were slightly more stable against SDS than process stress dimers (only 80 % of dimers dissociated into monomer molecules) and addition of DTT, which is reducing intra- and intermolecular disulfide bonds, led to complete dissociation of pH stress dimers into LC and HC (Fig. 4). TEM electron micrographs revealed a small 'close' conformation of the pH stress dimers, where two antibody molecules were attached to each other via two interaction sites. The two intermolecular association sites are likely the reason for the higher stability of these dimers in e.g. SDS buffer compared to process stress dimers, which expose only one intermolecular binding site. The schematic model of pH stress dimers is shown in Fig. 10b. To some extent, the two interaction sites in pH stress dimers were likely formed by Fab domains as determined for process stress dimers, but also the Fc region is possibly involved in the formation of the ring-like pH stress dimer conformation. The latter is speculated because apart from the additional Fab-dimer peak observed after IEC analysis of the papain fragments, the intensity of the monomeric Fc fraction was reduced (Fig. 6b). Interestingly, Fab-Fab interaction in process stress dimers led to reduced bioactivity / antigen-binding (62 % compared to monomer), while interaction in pH stress dimers did not impair bioactivity / binding to antigen (Table II, Fig. 8). In principle, partial dissociation of process and pH stress dimers could have occurred during bioassay analysis, but this is unlikely since pH stress dimers were more stable than process stress dimers. Moreover, the bioassay results could be confirmed with SPR binding assays: the higher bioactivity of pH stress dimers compared to process stress dimers correlated with higher binding affinity of the pH stress dimers towards the antigen (data not shown). It may be speculated that the CDR domains within the Fab part of pH stress dimers are still accessible because the Fab domains are associated together at another position as compared to process stress dimers and/or because the domains are attached to each other forming a tilted angle and therefore no steric hindrance occurs that impairs antigen binding. Because of the 'close' conformation of the pH stress dimer molecules these dimers had a smaller size according to TEM compared to process stress dimers (Fig. 7c). Notably, the size differences observed by TEM correlated well with the differences in the hydrodynamic diameters determined by SEC (Fig. 1). Accordingly, AUC data showed that the pH stress dimer had the most compact shape (the lowest frictional ratio) of the three stress-induced dimers (Fig. 2). The 'close' conformation moreover had a strong impact on the exposed hydrophobic surface of pH stress dimers, resulting in species which were significantly more hydrophobic as compared to the process stress dimers (Supplementary Material Figure S1). With regard to FcγRIIIa-binding the pH stress dimer was more heterogeneous, indicating that they contain a mixture of molecules with different numbers of active binding sites and/or different binding affinities.

Characterization of Light Stress Dimers

Light stress dimers were the most heterogeneous dimer species of all three dimer types. In contrast to process and pH stress dimers, the intensive exposure to UV light to generate light stress aggregates led to significant chemical modifications within the primary structure. Especially oxidation of methionine residues was detected (Fig. 3) which is a known chemical reaction due to photo-stress (24). Furthermore some chemical modifications which could not be identified were detected (see "unknown peaks" in Fig. 3). The high stability of light stress dimers against SDS (with or without DTT) indicated the formation of new inter- or intramolecular chemical bonds in these aggregates. According to literature, photo-degradation of an antibody may induce miscellaneous physical and chemical reactions including peptide bond cleavage, chemical cross-linking, fragmentation at the hinge region, oxidation of tryptophan and histidine residues (45,46) and deamidation reactions (24,47).

Therefore, a variety of other chemical modifications may be present in light stress dimers but could not be detected in

the peptide map most likely because the various chemical modifications would lead to a heterogeneous mixture of peptides which are distributed into several peaks of low intensities or are too complex to be identified (see unknown peaks in Fig. 3). In fact, a broad distribution of peaks was found for light stress dimers by IEC and HIC (data not shown) which also indicated that these aggregates were composed of a multitude of different species. Despite the strong chemical denaturation, the overall antibody Y-shape within light stress dimers could clearly be identified by negative stain TEM imaging. Therefore, the majority of the secondary and also tertiary structures of antibody molecules seemed to be unaffected by the light stress and by the dimerization process, as it was also found for the other stress induced dimers. This may explain why even in light stress dimers no structural alterations were detected by FTIR spectroscopy. Light stress dimers were very heterogeneous in their conformations, e.g. besides bone-like conformations also 'bended bones', 'sandwich-like' or 'close' conformations could be observed by TEM imaging. The average size of light stress dimers was between process and pH stress dimers according to TEM which is in good agreement to the intermediate hydrodynamic diameter as determined by SEC (Fig. 1) and the intermediate compactness (frictional coefficient) as determined by AUC (Fig. 2). Light stress dimers were mostly inactive in the potency assay (Table II, Fig. 8) and the remaining bioactivity can be attributed to the residual monomeric antibody present in the light stress dimer fraction. It is likely that especially the strong chemical modifications together with the dimerization led to the reduced binding affinity of light stress dimers towards the antigen. Also the function of the Fc region was partially impaired because the relative binding affinity determined in the FcγRIIIa-binding assay (Table III) was lower for light stress dimers in comparison to the other dimer types.

CONCLUSION

Protein aggregation is often investigated using stressed protein solutions containing a mixture of monomer and different soluble and/or insoluble aggregate species (17,20,24). In such mixtures the intrinsic characteristics of the aggregate molecules can hardly be discriminated from other molecules, because all present species contribute to the analytical result. The work described here demonstrates the potential of combining several analytical methodologies to study the structure-function relationship of enriched monoclonal antibody dimers generated by different stress conditions and purified by preparative chromatography. Thereby, it enables characterization of specific structures and *in vitro* activities of the dimer species in comparison to monomer. We have shown that the process, pH and light stress individually generated three different kinds of dimers with respect to their biophysical, biochemical, structural and bioactivity profiles. It is important to note that these observations were made for one monoclonal IgG1 antibody. Although IgG1 antibodies display a high degree of similarities, other IgG1 antibodies may form different dimer species. Our study shows that the combination of a full set of complementary methods for analysis of the purified species allows detailed insight into the structure of antibody aggregates and conclusion on the molecular architecture of aggregate species. Since such structural differences obviously have a strong impact on bioactivity, they might also be important for the safety and efficacy of the drug and should therefore be thoroughly assessed. The use of such defined and thoroughly characterized aggregate species should also be considered for immunogenicity research in order to address the question which specific types and amounts of aggregates may induce an immunogenic effect.

ACKNOWLEDGMENTS & DISCLOSURES

We thank Thomas von Hirschheydt, Marc Pompiati, Gordan Graf (all Roche Penzberg) and Marco Sonderegger for their support in isolation of aggregates. We sincerely acknowledge Rita Grübel, Gaby Walch, Jürgen May, Bernd Moritz, Stephen Hyland, Philipp Metzger, Jörg Hoernschemeyer and Eric Kusznir for their contributions to analytical characterizations of the dimers. Thanks to Jochem Alsenz and Michael Hennig for supporting the TEM experiments. We acknowledge Thomas Schreitmueller for sponsoring and supporting the project. This work was in part supported by the Swiss initiative for systems biology (SystemsX.ch).

REFERENCES

1. Hermeling S, Crommelin DJA, Schellekens H, Jiskoot W. Structure–immunogenicity relationships of therapeutic proteins. Pharm Res. 2004;21:897–903.
2. Rosenberg AS. Effects of protein aggregates: an immunologic perspective. AAPS J. 2006;8:501–7.
3. Kumar S, Singh SK, Wang X, Rup B, Gill D. Coupling of aggregation and immunogenicity in biotherapeutics: T- and B-cell immune epitopes may contain aggregation-prone regions. Pharm Res. 2011;28(5):949–61.
4. Philo JS. Is any measurement method optimal for all aggregate sizes and types? AAPS J. 2006;8(3):E564–71.
5. Cao S, Jiao N, Jiang Y, Mire-Sluis A, Narhi L. Sub-visible particle quantitation in protein therapeutics. Pharmeur Bio Sci Notes. 2009;2009(1):73–9.
6. Singh SK, Afonina N, Awwad M, Bechtold-Peters K, Blue JT, Chou D, *et al.* An industry perspective on the monitoring of subvisible particles as a quality attribute for protein therapeutics. J Pharm Sci. 2010;99(8):3302–21.
7. den Engelsman J, Garidel P, Smulders R, Koll H, Smith B, Bassarab S, *et al.* Strategies for the assessment of protein aggregates in pharmaceutical biotech product development. Pharm Res. 2011;28(4):920–33.

8. Bond MD, Panek ME, Zhang Z, Wang D, Mehndiratta P, Zhao H, *et al.* Evaluation of a dual-wavelength size exclusion HPLC method with improved sensitivity to detect protein aggregates and its use to better characterize degradation pathways of an IgG1 monoclonal antibody. J Pharm Sci. 2010;99(6):2582–97.
9. Zhang A, Singh SK, Shirts MR, Kumar S, Fernandez EJ. Distinct aggregation mechanisms of monoclonal antibody under thermal and freeze-thaw stresses revealed by hydrogen exchange. Pharm Res. 2012;29(1):236–50.
10. Chi EY, Krishnan S, Randolph TW, Carpenter JF. Physical stability of proteins in aqueous solution: mechanism and driving forces in nonnative protein aggregation. In: Pharmaceutical Research: Springer Netherlands; 2003. p. 1325–1336.
11. Cromwell M, Hilario E, Jacobson F. Protein aggregation and bioprocessing. AAPS J. 2006;8:E572–9.
12. Van Buren N, Rehder D, Gadgil H, Matsumura M, Jacob J. Elucidation of two major aggregation pathways in an IgG2 antibody. J Pharm Sci. 2009;98(9):3013–30.
13. Mahler H-C, Friess W, Grauschopf U, Kiese S. Protein aggregation: pathways, induction factors and analysis. J Pharm Sci. 2009;98 (9):2909–34.
14. Hermeling S, Schellekens H, Maas C, Gebbink MF, Crommelin DJ, Jiskoot W. Antibody response to aggregated human interferon alpha2b in wild-type and transgenic immune tolerant mice depends on type and level of aggregation. J Pharm Sci. 2006;95(5):1084–96.
15. van Beers M, Sauerborn M, Gilli F, Brinks V, Schellekens H, Jiskoot W. Aggregated Recombinant Human Interferon Beta Induces Antibodies but No Memory in Immune-Tolerant Transgenic Mice. In: Pharmaceutical Research: Springer Netherlands; 2010. p. 1812–1824.
16. Fradkin AH, Carpenter JF, Randolph TW. Immunogenicity of aggregates of recombinant human growth hormone in mouse models. J Pharm Sci. 2009;98(9):3247–64.
17. Kiese S, Papppenberger A, Friess W, Mahler H-C. Shaken, not stirred: mechanical stress testing of an IgG1 antibody. J Pharm Sci. 2008;97(10):4347–66.
18. Mahler H-C, Müller R, Friess W, Delille A, Matheus S. Induction and analysis of aggregates in a liquid IgG1-antibody formulation. Eur J Pharm Biopharm. 2005;59(3):407–17.
19. Hawe A, Kasper JC, Friess W, Jiskoot W. Structural properties of monoclonal antibody aggregates induced by freeze-thawing and thermal stress. Eur J Pharm Sci. 2009;38(2):79–87.
20. Joubert MK, Luo Q, Nashed-Samuel Y, Wypych J, Narhi LO. Classification and characterization of therapeutic antibody aggregates. J Biol Chem. 2011;286(28):25118–33.
21. Remmele RL, Callahan WJ, Krishnan S, Zhou L, Bondarenko PV, Nichols AC, *et al.* Active dimer of Epratuzumab provides insight into the complex nature of an antibody aggregate. J Pharm Sci. 2006;95(1):126–45.
22. Ejima D, Tsumoto K, Fukada H, Yumioka R, Nagase K, Arakawa T, *et al.* Effects of acid exposure on the conformation, stability, and aggregation of monoclonal antibodies. Proteins Struct Funct Bioinforma. 2007;66(4):954–62.
23. Perico N, Purtell J, Dillon TM, Ricci MS. Conformational implications of an inversed pH-dependent antibody aggregation. J Pharm Sci. 2009;98(9):3031–42.
24. Qi P, Volkin DB, Zhao H, Nedved ML, Hughes R, Bass R, *et al.* Characterization of the photodegradation of a human IgG1 monoclonal antibody formulated as a high-concentration liquid dosage form. J Pharm Sci. 2009;98(9):3117–30.
25. Schuck P. On the analysis of protein self-association by sedimentation velocity analytical ultracentrifugation. Anal Biochem. 2003; 320(1):104–24.
26. Kendall A, McDonald M, Stubbs G. Precise determination of the helical repeat of tobacco mosaic virus. Virology. 2007;369(1):226–7.
27. Ludtke SJ, Baldwin PR, Chiu W. EMAN: semiautomated software for high-resolution single-particle reconstructions. J Struct Biol. 1999;128(1):82–97.
28. Byler DM, Susi H. Examination of the secondary structure of proteins by deconvolved FTIR spectra. Biopolymers. 1986;25(3):469–87.
29. Dong A, Huang P, Caughey W. Protein secondary structures in water from second-derivative amide I infrared spectra. Biochemistry. 1990;29(13):3303–8.
30. Lau H, Pace D, Yan B, McGrath T, Smallwood S, Patel K, *et al.* Investigation of degradation processes in IgG1 monoclonal antibodies by limited proteolysis coupled with weak cation-exchange HPLC. J Chromatogr B. 2010;878(11–12):868–76.
31. Harris LJ, Skaletsky E, McPherson A. Crystallographic structure of an intact IgG1 monoclonal antibody. J Mol Biol. 1998;275(5):861–72.
32. Roux KH. Immunoglobulin structure and function as revealed by electron microscopy. Int Arch Allergy Immunol. 1999;120:85–99.
33. Bongini L, Fanelli D, Piazza F, De Los Rios P, Sandin S, Skoglund U. Freezing immunoglobulins to see them move. Proc Natl Acad Sci U S A. 2004;101(17):6466–71.
34. Roux K, Strelets L, Michaelsen T. Flexibility of human IgG subclasses. J Immunol. 1997;159(7):3372–82.
35. Demeule B, Palais C, Machaidze G, Gurny R, Arvinte T. New methods allowing the detection of protein aggregates: a case study on trastuzumab. MAbs. 2009;1(2):142–50.
36. Taschner N, Müller SA, Alumella VR, Goldie KN, Drake AF, Aebi U, *et al.* Modulation of antigenicity related to changes in antibody flexibility upon lyophilization. J Mol Biol. 2001;310(1):169–79.
37. Kanai S, Liu J, Patapoff TW, Shire SJ. Reversible self-association of a concentrated monoclonal antibody solution mediated by Fab-Fab interaction that impacts solution viscosity. J Pharm Sci. 2008;97 (10):4219–27.
38. Moore JMR, Patapoff TW, Cromwell MEM. Kinetics and thermodynamics of dimer formation and dissociation for a recombinant humanized monoclonal antibody to vascular endothelial growth factor. Biochemistry. 1999;38(42):13960–7.
39. Dall'Ozzo S, Tartas S, Paintaud G, Cartron G, Colombat P, Bardos P, *et al.* Rituximab-dependent cytotoxicity by natural killer cells: influence of FCGR3A polymorphism on the concentration-effect relationship. Cancer Res. 2004;64(13):4664–9.
40. Ferrara C, Brunker P, Suter T, Moser S, Puntener U, Umana P. Modulation of therapeutic antibody effector functions by glycosylation engineering: influence of Golgi enzyme localization domain and co-expression of heterologous beta1, 4-N-acetylglucosaminyltransferase III and Golgi alpha-mannosidase II. Biotechnol Bioeng. 2006;93 (5):851–61.
41. Lewis JD, Ju RTC, Kim AI, Nail SL. Kinetics of low pH induced aggregation of equine IgG. J Colloid Interface Sci. 1997;196 (2):170–6.
42. Hari SB, Lau H, Razinkov VI, Chen S, Latypov RF. Acid-induced aggregation of human monoclonal IgG1 and IgG2: molecular mechanism and the effect of solution composition. Biochemistry. 2010;49(43):9328–38.
43. Vermeer AW, Norde W. The thermal stability of immunoglobulin: unfolding and aggregation of a multi-domain protein. Biophys J. 2000;78(1):394–404.
44. Brummitt RK, Nesta DP, Chang L, Chase SF, Laue TM, Roberts CJ. Nonnative aggregation of an IgG1 antibody in acidic conditions: part 1. Unfolding, colloidal interactions, and formation of high-molecular-weight aggregates. J Pharm Sci. 2011;100(6):2087–103.
45. Liu H, Gaza-Bulseco G, Faldu D, Chumsae C, Sun J. Heterogeneity of monoclonal antibodies. J Pharm Sci. 2008;97(7):2426–47.
46. Kerwin BA, Remmele RL. Protect from light: photodegradation and protein biologics. J Pharm Sci. 2007;96(6):1468–79.
47. Huang L, Lu J, Wroblewski VJ, Beals JM, Riggin RM. *In vivo* deamidation characterization of monoclonal antibody by LC/MS/MS. Anal Chem. 2005;77(5):1432–9.